Unambiguous Recovery of Multistatic SAR Datafor Nonzero Cross Track Baseline Case

Dogan, O.; Uysal, Faruk; Lopez Dekker, J.F.

DOI
10.1109/LGRS.2020.3021759

Publication date
2020

Document Version
Accepted author manuscript

Published in
IEEE Geoscience and Remote Sensing Letters

Unambiguous Recovery of Multistatic SAR Data for Nonzero Cross Track Baseline Case

Ozan Dogan, Faruk Uysal, *Senior Member, IEEE*, and Paco Lopez Dekker, *Senior Member, IEEE*

***Abstract*— A wide-swath synthetic aperture radar (SAR) image is known to be achievable by merging multistatic aliased data that is collected with an appropriate along-track displacement. However, in terms of both flexibility requirements like potentiality of both along-track and cross-track (XT) interferometry and design requirements like orbital safety, etc., a XT baseline is not only demanded but also unavoidable. In this work, a method is proposed in order to merge SAR data to recover the Doppler spectrum unambiguously for the nonzero XT baseline case. The algorithm is compared and validated by simulating an azimuth invariant multistatic SAR satellite constellation. The results are promising in terms of dealing with XT baselines.**

***Index Terms*— Bistatic synthetic aperture radar (SAR), multistatic SAR image processing, radar signal processing, SAR constellation.**

I. Introduction

THE state of the art for bistatic synthetic aperture radar (SAR) imaging is quite mature [1], [2], [5]. Currently, the frequency spectrum of the bistatic SAR signal is already derived [6], the problem is mathematically well investigated to convert the bistatic measurement to a monostatic one [7], bistatic SAR image formation algorithms are proposed [8], [9], and validated with the airborne [10] and spaceborne experiments [11]. These works are limited to the spatially distinguished single transmitter and single receiver case.

The next generation of spaceborne SAR system is demanded to support product diversity, for example, high-resolution wide-swath (HRWS) imaging, along-track and cross-track (XT) interferometry, and so on. Another trend is the low-cost small satellites that have smaller antennas which means wide beamwidths and higher azimuth ambiguity power. Conventional SAR systems cannot meet the HRWS imaging requirement due to the fact that the unambiguous swath width and achievable azimuth resolution pose contradicting requirements on system design [10]. To overcome this limitation, a multistatic SAR reconstruction method for along-track displaced passive receivers is already proposed [12]. There are further advancements in this method to deal with higher nonuniform sampling case [3], [13] and error calibration [14].

Manuscript received February 25, 2020; revised July 16, 2020 and August 12, 2020; accepted September 1, 2020. This work was supported by the Netherlands Organisation for Scientific Research (NWO) through the Dutch Knowledge Network on Radar Instruments and Applications (NL-RIA) Project. *(Corresponding author: Ozan Dogan.)*

Ozan Dogan and Faruk Uysal are with EEMCS, Delft University of Technology, 2628 Delft, The Netherlands (e-mail: o.dogan@tudelft.nl).

Paco Lopez Dekker is with CiTG, Delft University of Technology, 2628 Delft, The Netherlands.

Color versions of one or more of the figures in this letter are available online at http://ieeexplore.ieee.org.

Digital Object Identifier 10.1109/LGRS.2020.3021759

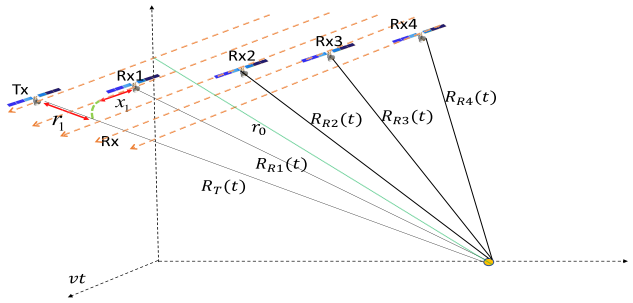

Fig. 1. Multistatic SAR geometry—single transmitter and four receivers.

To the best of our knowledge, the effort for combining multiple bistatic SAR data for the HRWS imaging is limited to merely along-track baselines. There are some efforts for combining monostatic SAR images for very short XT baselines [4], [15], and in the case of topography deviation [16]. In practice, the existence of XT baselines may be intentional for single-pass XT interferometry, orbital safety or maybe unintentional due to orbital accuracy. So an XT baseline is, strictly speaking, unavoidable and must be compensated in order to merge multistatic data in an alias free manner.

There are different methods in the literature for combining multistatic SAR data [17], [18]. However, these works are not motivated to extract HRWS images by using a low pulse repetition frequency (PRF) signal.

In this work, the multistatic SAR image formation problem for the nonzero XT baseline under the assumption of flat earth is investigated and mathematically modeled for the low squint case. Based on this derivation, a linear transformation will be derived for converting a multistatic SAR signal to a single reference measurement. The simulation results show that the proposed method performs well for suppressing the azimuth ambiguities.

II. Problem Definition

A. Single Target Case

The multistatic SAR constellation, illustrated in Fig. 1, consists of a single transmitter that illuminates a point target while multiple receivers collect the backscattered data in broadside geometry. The orbits are azimuth invariant; the synthetic aperture is sufficiently short that the relative movement between the satellites is negligible. The along-track and XT line of sight baseline between the transmitter and the ith receiver is shown as x_i and r_i, respectively. We note that the XT line of sight baseline is a function of perpendicular and parallel baselines

that any of them can be nonzero. The received multistatic SAR raw data for a single point target can be written as follows:

$$\begin{aligned} s_{ri}(t,\eta,r_0,\eta_0) = {} & A_{\mathrm{Tx}}(\eta)A_{\mathrm{Rx},i}(\eta) \\ & \times \mathrm{rect}\left(\frac{t}{\tau}-\frac{R_i(r_0,\eta)}{\tau c}\right)e^{-j2\pi R_i(r_0,\eta)/\lambda} \\ & \times \gamma(r_0,\eta_0)e^{j\pi\alpha_r\left(t-\frac{R_i(r_0,\eta)}{c}\right)^2} \end{aligned} \tag{1}$$

where

$$\begin{aligned} R_i(r_0,\eta) &= \sqrt{r_0^2+v^2\eta^2}+\sqrt{(r_0-r_i)^2+(v\eta-x_i)^2} \\ &= R_T(r_0,\eta)+R_{R_i}(r_0,\eta) \end{aligned} \tag{2}$$

is the bistatic range, $\gamma(r_0,\eta_0)$ is the reflectivity of the target at the range position r_0 and azimuth time η_0 (which is equal to zero for the broadside geometry), t is the fast time, α_r is the chirp rate of the transmitted linear frequency modulated signal, rect is representing the rectangular shape of the pulse, τ is the pulsewidth, η is the azimuth time, $R_i(r_0,\eta)$ is the range in the bistatic geometry, R_T is the range between the transmitter and the target, and $R_{R_i}(r_0,\eta)$ is the range between the ith receiver and the target, A_{Tx} and $A_{\mathrm{Rx},i}$ define the envelope of the azimuth signal arising from the projection of the transmit and receive antenna patterns on the ground. The elevation beamwidth of the antenna is assumed to be sufficiently wide and so is not included in the equation.

The overall slant range histories lose their hyperbolic form since the sum of two hyperbolas is no longer a hyperbola as it is expressed in (2). Thus, slant range histories look different (the shape is flattened; a flat-top hyperbola) from the receiver slant range history [6].

Note that receivers are assumed to be synchronized in time and frequency with the transmitter. The power of each signal is assumed to be the same since the range and angle of each satellite are identical and hardware-based difference can be compensated [19].

The Taylor Series expansion of the bistatic range equation up to the quadratic term are known to be a valid approximation for the low squint cases [21], and can be written as follows:

$$R_i(r_0,\eta) = R_i(r_0\eta_{0_i}) + \frac{\lambda\alpha_i(r_0)}{2}(\eta-\eta_{0_i})^2+\cdots \tag{3}$$

where the azimuth chirp rate is

$$\begin{aligned} \alpha_i(r_0) = \frac{v^2}{\lambda}\Bigg[& \frac{1}{R_T(r_0,\eta_{0_i})}\left(1-\frac{v^2\eta_{0_i}^2}{R_T(r_0,\eta_{0_i})^2}\right) \\ & +\frac{1}{R_R(r_0,\eta_{0_i})}\left(1-\frac{v^2\eta_{0_i}^2}{R_R(r_0,\eta_{0_i})^2}\right)\Bigg] \end{aligned} \tag{4}$$

and bistatic range, $R_i(r_0,\eta_{0_i})$, can be written as

$$R_i(r_0,\eta_{0_i}) \approx 2r_0 - r_i + \frac{x_i^2}{2(2r_0-r_i)}. \tag{5}$$

The azimuth time of the target that has zero Doppler frequency is derived as (see Appendix)

$$\eta_{0_i} = \frac{r_0 x_i}{v(2r_0-r_i)}. \tag{6}$$

For optimum performance, the along-track displacement of the subapertures $i=2,\ldots,N$ relative to the first receiver $i=1$ should be selected as

$$\eta_{0_i} = \frac{r_0 x_i}{v(2r_0-r_i)} \approx \frac{1}{\mathrm{PRF}}\left(\frac{i-1}{N}+k_i\right) \tag{7}$$

where N is the number of satellites. Such a scheme results in a uniform sampling of the received SAR signal. We note that for $r_i=0$, this expression is the same as is given in [10], [12], and [20].

The intended multistatic mission scope in this letter is a swarm SAR concept that the width of the along-track separation of the satellites is short enough to fulfill the low squint requirement for the broadside geometry case. So the classical range Doppler algorithm (RDA), which is based on the range approximation according to the Taylor series expansion, can potentially form the multistatic SAR image by using the range compression (RC) and the range cell migration correction (RCMC).

The range compressed signal can be written as follows:

$$\begin{aligned} s_{rc_i}(t,\eta) = {} & A_{\mathrm{Tx}}(\eta)A_{\mathrm{Rx},i}(\eta) \\ & \times \gamma(r_0,\eta_0)\tau e^{-j2\pi R_i(r_0,\eta)/\lambda} \\ & \times \mathrm{sinc}(\alpha_r\tau(t-R_i(r_0,\eta)/c)). \end{aligned} \tag{8}$$

For the squinted case, one may take into consideration the secondary RC as is discussed for the bistatic case [9]. Next is the RCMC step. The RCMC can be implemented as an interpolation (or a phase multiplication in Fourier Domain) with the range $R_i(r_0,\eta)$ defined in (2) to $R_i(\eta_0)$ defined in (5) except instead of r_0 we insert $c\eta/2$ in both equations. The RCMC output of the signal can be expressed as follows:

$$\begin{aligned} s_{rcmc_i}(t,\eta,r_0,\eta_0) = {} & A_{\mathrm{Tx}}(\eta)A_{\mathrm{Rx},i}(\eta) \\ & \times\gamma(r_0,\eta_0)\tau e^{-j2\pi R_i(r_0,\eta)/\lambda} \\ & \times \mathrm{sinc}(\alpha_r\tau(t-R_i(r_0,\eta_{0_i})/c)) \end{aligned} \tag{9}$$

$$= \gamma(r_0,\eta_0)s_i(t,\eta,r_0,\eta_0) \tag{10}$$

where $s_i(t,\eta,r_0,\eta_0)$ is the impulse response of the SAR system. Hence, for the multistatic SAR case.

1) The RCMC output of different orbits are shifted in fast time corresponding to the range, $R_i(r_0,\eta_{0_i})$ given in (5).
2) If the radar pulse instants of each satellite combination are not synchronized but known, the additional fast time shift can be compensated in the RCMC step.
3) The power of the signal is related to the difference between the target range time and the sampling time resulting in channel imbalance within receivers and must be calibrated.
4) The RCMC is applied to the undersampled data that limit, δ_a, the azimuth resolution as: $(vN_{\mathrm{sat}})/\mathrm{PRF} < \delta_a$.

Once there is a single target at a known position, a phase compensation term can be derived simply by following the steps in [12] and [22] including the XT baseline and final azimuth compression can be used for SAR imaging. This method does not work in the extended scene case as the compensation term is calculated for a specific position of the target for the nonzero XT case.

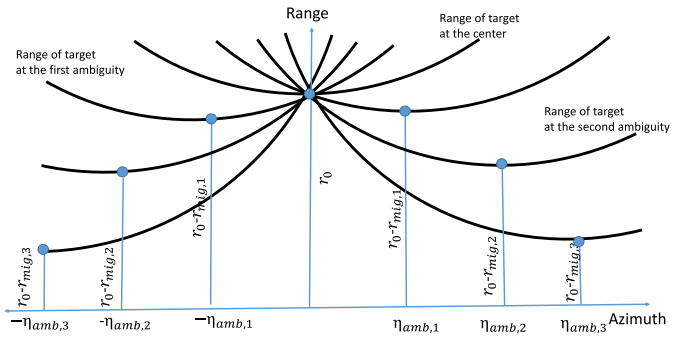

Fig. 2. Range of targets. The ambiguous targets and the unambiguous target.

B. Extended Scene-Single Satellite Case

The geometry of the problem is much more complicated for the extended scene case as far as the nonzero XT baseline is concerned. Let us start with a single satellite. Suppose that, there is a single target of interest at the broadside position, $(r_0, \eta_0 = 0)$. For this case, the radar range versus azimuth time is illustrated in Fig. 2. The radar range of another target at the position of $(r_0 - r_{\mathrm{mig}_1}, \eta_{\mathrm{amb}_1})$, that η_{amb_1} is the first azimuth ambiguity, intersects the radar range of the target at the target of interest; thus contributes to the signal due to aliasing. The same situation is the case for the target at complimentary ambiguity, $(r_0 - r_{\mathrm{mig}_1}, -\eta_{\mathrm{amb}_1})$. Nevertheless, the received data corresponding to a single target at the azimuth center for the Nyquist rate compatible PRF case is the summation of aliased signals backscattered from multiple targets at the position of ambiguities and the target of interest at the center. This summation can be expressed mathematically as follows:

$$S_i(t,\eta) = \sum_{k=-N_{\mathrm{amb}}}^{N_{\mathrm{amb}}} \gamma\left(r_0 - r_{\mathrm{mig}_k}, \eta_{\mathrm{amb}_k}\right) \times s_i\left(t, \eta, r_0 - r_{\mathrm{mig}_k}, -\eta_{\mathrm{amb}_k}\right) \quad (11)$$

where r_{mig_k} is the migration in range with respect to the target of interest and η_{amb_k} is the azimuth ambiguity, explicitly

$$\eta_{\mathrm{amb}_k} = \frac{\mathrm{PRF}}{2\alpha_k}, \quad r_{\mathrm{mig}_k} = r_{\mathrm{mig}_{-k}} \approx \alpha_k \frac{\lambda \eta_{\mathrm{amb}_k}^2}{4}. \quad (12)$$

Here, the Taylor series expansion up to the quadratic term is sufficient for the estimation of ambiguities and valid for the narrow beam broadside geometry. This assumption results in the case that the azimuth time of the ambiguities are the multitudes of the first one, $\eta_{\mathrm{amb}_k} = k\eta_{\mathrm{amb}_1}$.

C. Extended Scene-Multiple Satellite Case

In (11), it is formulated that the received signal is a summation of multiple ambiguities and the signal backscattered from the target at the broadside direction. The number of unknowns for the reflectivity $\gamma\left(r_0 \quad - r_{\mathrm{mig}_k}, \eta_{\mathrm{amb}_k}\right)$ is $2N_{\mathrm{amb}} + 1$. Thus, a system of linear equations can be obtained by using $N = 2N_{\mathrm{amb}} + 1$ satellites as in (14), shown at the bottom of the page. In the vector notation (14) can be written as

$$\mathbf{S} = \mathbf{H\Gamma} \quad (13)$$

where $\mathbf{S} = [S_1, S_2, \ldots, S_N]$ is the received signal of multiple satellites, $\mathbf{H}$ is the impulse response function, $H_{i,k} = s_i(t, \eta, r_0 - r_{\mathrm{mig}_k}, \eta_{\mathrm{amb}_k})$ and $\mathbf{\Gamma}$ is the reflectivity of the target.

III. Method

The system defined by (14) is an "underdetermined" system as far as infinite number of ambiguities are taken into consideration. The proposed method can handle N_{amb} ambiguities in the case of $N = 2N_{\mathrm{amb}} + 1$ satellites. We define the impulse response of each ambiguity as follows:

$$\begin{aligned} s_{ik} &= s_i(t, \eta, r_0 - r_{\mathrm{mig}_k}, \eta_{\mathrm{amb}_k}) \\ &= A_{ik}(r_0 - r_{\mathrm{mig}_k}, \eta) \\ &\quad \times e^{-j2\pi R_i(r_0 - r_{\mathrm{mig}_k}, \eta_{0_i})/\lambda} \\ &\quad \times e^{(j\pi\alpha_i(r_0 - r_{\mathrm{mig}_k})(\eta - \eta_{0_i} - \eta_{\mathrm{amb}_k})^2)} \end{aligned} \quad (15)$$

where A_{ik} represents the beam of the antenna pattern corresponding to the kth ambiguity or the broad side one for $k = 0$, the first exponential is the phase shift and the second exponential includes the linear frequency modulation in azimuth direction.

To transfer the collected data from different satellites to a reference origin, the inverse of the system transfer function $\mathbf{H^{-1}}$ will be estimated and multiplied with the desired impulse response of the system

$$\mathbf{s'} = \mathbf{H_c H^{-1} s_r} \quad (16)$$

where $H_{i1} = s_{i0}$, $H_{ik} = s_{ij}$, $j = (-1)^{k-1}\lfloor k/2 \rfloor$, and H_c is the impulse response matrix generated by the geometry of the first bistatic measurement as reference: $H_c = H|_{i=1}$.

The flow of the proposed multistatic SAR image formation algorithm is shown in (Fig. 3). The algorithm flow begins with the RC and RCMC. Next, signal is shifted in range to compensate the time shift due to nonzero cross track baseline. The next step is the compensation of the phase difference that corresponds to the range difference between the acquisitions according to (5). The channel calibration is done to eliminate

$$s_r(t,\eta) = \begin{bmatrix} s_1(t,\eta,r_0,0) & s_1(t,\eta,r_0 - r_{\mathrm{mig}_1}, -\eta_{\mathrm{amb}_1}) & s_1(t,\eta,r_0 - r_{\mathrm{mig}_1}, \eta_{\mathrm{amb}_1}) & . & . \\ s_2(t,\eta,r_0,0) & s_2(t,\eta,r_0 - r_{\mathrm{mig}_1}, -\eta_{\mathrm{amb}_1}) & s_2(t,\eta,r_0 - r_{\mathrm{mig}_1}, \eta_{\mathrm{amb}_1}) & . & . \\ . & . & . & . & . \\ s_N(t,\eta,r_0,0) & s_N(t,\eta,r_0 - r_{\mathrm{mig}_1}, -\eta_{\mathrm{amb}_1}) & s_N(t,\eta,r_0 - r_{\mathrm{mig}_1}, \eta_{\mathrm{amb}_1}) & . & . \end{bmatrix} \begin{bmatrix} \gamma(r_0, 0) \\ \gamma(r_0 - r_{\mathrm{mig}_1}, -\eta_{\mathrm{amb}_1}) \\ \gamma(r_0 - r_{\mathrm{mig}_1}, \eta_{\mathrm{amb}_1}) \\ . \\ \gamma(r_0 - r_{\mathrm{mig}_{N_{\mathrm{amb}}}}, \eta_{\mathrm{amb}_{N_{\mathrm{amb}}}}) \end{bmatrix} \quad (14)$$

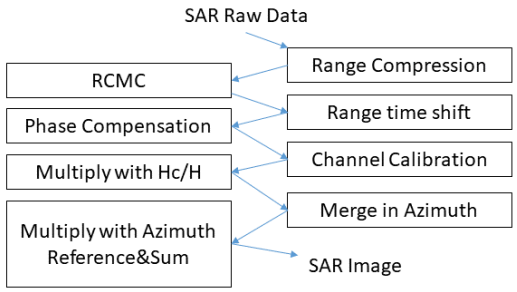

Fig. 3. Multistatic SAR image formation algorithm flow.

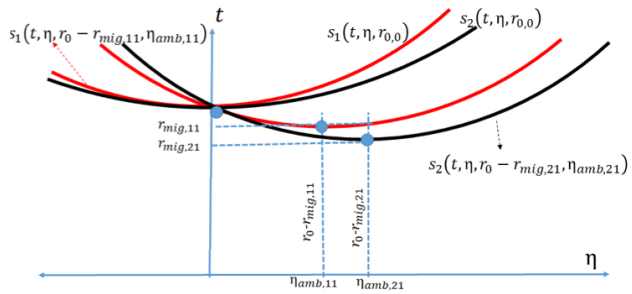

Fig. 4. Range migration and ambiguity difference in two satellite case for the nonzero XT baseline.

the difference of the amplitude for multiple measurements. For higher bistatic angle or for the squinted cases, a further coregistration step may be included to the calibration step [23]. The multiplication with the H_c/H is done as in (16). Data are sorted in azimuth time and then the matched filtering is implemented by a multiplication with the N_{sat} times upsampled azimuth reference function and summation to obtain the final SAR image.

The final SAR image can be extracted by sorting the compensated signal, $\mathbf{s}'$, corresponding to the azimuth time shift, multiplying with the reference filter and summation.

A. Validity Limits

To validate the formulation of the problem and the proposed method, let us focus on two satellites with a nonzero XT baseline case. The chirp rates for this case will be different, resulting in a shift in both range and azimuth of the ambiguity as it is implicitly included in (4). To have a physical understanding of the problem, the flat top hyperbolas representing the range to a target in the scene center is drawn for two satellites in Fig. 4. Observe that the position of the first ambiguous target signature for two measurements are not at the same position. Hence, the targets that are contributing to the signal are displaced. In this case, the assumption made to formulate the problem in (13) is that the correlation length of the reflectivity is long enough to neglect the displacement of the ambiguity.

In order to show the performance limits of the proposed method, let us consider a case where this assumption is not valid and there is a nonignorable difference between the reflectivity of the targets. This difference represents an additional

TABLE I
SYSTEM PARAMETERS

Parameter	Value	Unit
Operating Frequency	3.2	GHz
Number of satellites	3	NA
Cross Track Baselines	0,250,500	m
Along Track Baselines	0,8.4,16.7	m
PRF	300	Hz
Effective Platform Velocity	7540	m/s
Band width	10	MHz
Pulse width	20	us
r_0	500	km

target for one of the N_{sat} measurements and contribute to the ambiguity with a power of at most half (in the two satellite case) of the power difference

$$\gamma_{\text{dB}}(r_0 - r_{\text{mig}_i}, \eta_{\text{amb}_i}) - \gamma_{\text{dB}}(r_0 - r_{\text{mig}_1}, \eta_{\text{amb}_1}) < \text{AASR}_{\text{min}} - 3 \text{ dB} \quad (17)$$

where AASR_{min} is the minimum acceptable azimuth ambiguity-to-signal ratio (AASR).

IV. RESULTS

To show the effectiveness of the proposed method, a multistatic spaceborne SAR system with nonzero XT baseline is simulated by using the system parameters in Table I. Antenna pattern is selected uniform not to bias the results since antenna pattern helps further suppression of the ambiguity. So a fair comparison of ambiguity to signal ratio can be achieved. The PRF is selected as the optimum value for the scene center according to (7).

The largest range migration difference for this experiment is computed $(v^2/2r_0)(\eta^2_{\text{amb}_3} - \eta^2_{\text{amb}_1}) = 0.87$ mm and ambiguity shift is $v(\eta_{\text{amb}_3} - \eta_{\text{amb}_1}) = 0.93$ m. Thus, for this geometry and system setup, the azimuth shift limits the correlation more.

First, a simulation with a single point scatterer is done. The first azimuth ambiguity to signal ratio (FAASR) is measured as -27 dB, a value that is quite reasonable for high quality SAR imaging in terms of suppression performance of the proposed method comparing with the single satellite case [10], and in addition in terms of 20 dB of SNR considerations [12] and typical 21 dB of dynamic range of SAR images. We note that for this geometry the measured FAASR for the proper sampled monostatic SAR experiment is -36 dB.

To verify the performance of the algorithm, a real SAR image that is extracted by TerraSAR-X is used as the reference reflectively for simulation purpose. The original SAR image is shown in Fig. 5 (left image), the simulated and processed SAR image for the single satellite case is shown in the middle and the SAR image obtained with the proposed method is shown in the right of Fig. 5. In all subfigures, vertical axis shows the index of ambiguities whereas the horizontal axis represents the range. The right figure shows that the proposed method performs quite good for suppression of the ambiguities. In the single satellite case, the ambiguities are distinctive for the high reflectivity scatterers.

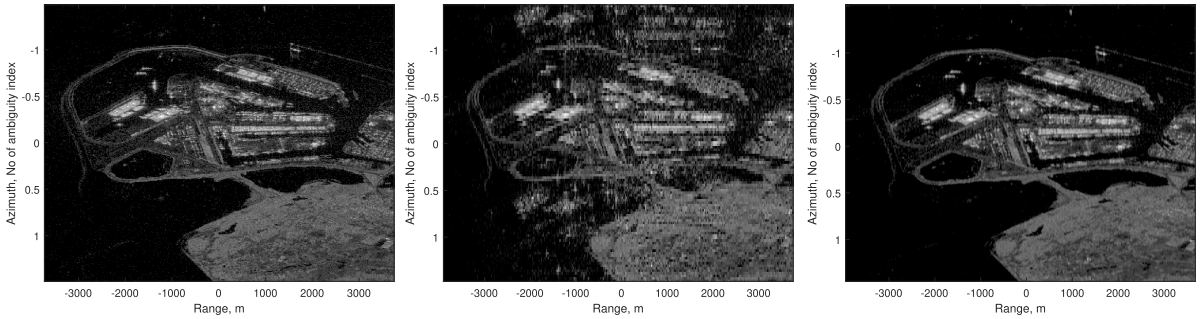

Fig. 5. (Left) Original SAR image from Port of Rotterdam (51°57'03.0"N 3°59'43.0"E). (Middle) Image of simulated single satellite case. (Right) Image of proposed method after merging of simulated three satellites' data. Vertical axis is the number of ambiguity, horizontal axis is the range.

V. Conclusion

In this letter, the problem of the multistatic SAR image formation algorithm for the nonzero XT baselines is defined geometrically. A mathematical approximation is proposed to achieve HRWS SAR imaging. The method can perform well in suppressing the ambiguities. The major limitations of the algorithm are the Taylor series expansion up to the quadratic term and correlation length of the reflectivity which both restricts the XT baseline.

Appendix

Bistatic range can be written as follows:

$$R_{\text{bistatic}}(\eta) = \sqrt{r_0^2 + v^2\eta^2} + \sqrt{(r_0 - r_i)^2 + (v\eta - x_i)^2}. \tag{18}$$

The Doppler frequency can be computed by taking the derivative of the range equation as

$$f = \frac{1}{\lambda}\left(\frac{v^2\eta}{\sqrt{r_o^2 + v^2\eta^2}} + \frac{v^2\eta - vx_i}{\sqrt{(r_0 - r_i)^2 + (v\eta - x_i)^2}}\right). \tag{19}$$

The azimuth time that makes Doppler to zero can be found as

$$\frac{v\eta}{\sqrt{r_o^2 + v^2\eta^2}} + \frac{v\eta - x_i}{\sqrt{(r_0 - r_i)^2 + (v\eta - x_i)^2}} = 0. \tag{20}$$

By solving (20), one can result in the following two solutions:

$$\eta_1 = \frac{r_0 x_i}{v r_i} \quad \text{and} \quad \eta_2 = \frac{r_0 x_i}{v(2r_0 - r_i)}. \tag{21}$$

These are the intersection points of two circles and the first is very far away from the current positions of the satellites while the second one is in the vicinity of midpoint of transmitter and the corresponding receiver. It is reasonable to use the second one to cover the case where there is a single intersection at $r_i = 0$. Thus, we define $\eta_{0_i} = \eta_2$.

References

[1] M. Cherniakov, *Bistatic Radar: Emerging Technology*. Hoboken, NJ, USA: Wiley, 2008.

[2] R. Wang and Y. Deng, *Bistatic SAR System and Signal Processing Technology*. New York, NY, USA: Springer, 2018.

[3] D. Cerutti-Maori, I. Sikaneta, J. Klare, and C. H. Gierull, "MIMO SAR processing for multichannel high-resolution wide-swath radars," *IEEE Trans. Geosci. Remote Sens.*, vol. 52, no. 8, pp. 5034–5055, Aug. 2014.

[4] P. Guccione, A. M. Guarnieri, F. Rocca, D. Giudici, and N. Gebert, "Along-track multistatic synthetic aperture radar formations of minisatellites," *Remote Sens.*, vol. 12, no. 1, p. 124, Jan. 2020.

[5] M. Rodriguez-Cassola, P. Prats-Iraola, G. Krieger, A. Reigber, and A. Moreira, "Bistatic SAR image formation: A systematic approach," in *Proc. IEEE Geosci. Remote Sens. Symp.*, Jul. 2014, pp. 3945–3948.

[6] O. Loffeld, H. Nies, V. Peters, and S. Knedlik, "Models and useful relations for bistatic SAR processing," *IEEE Trans. Geosci. Remote Sens.*, vol. 42, no. 10, pp. 2031–2038, Oct. 2004.

[7] A. M. Guarnieri and F. Rocca, "Reduction to monostatic focusing of bistatic or motion uncompensated SAR surveys," *IEE Proc.-Radar, Sonar Navigat.*, vol. 153, no. 3, p. 199, 2006.

[8] Y. L. Neo, F. Wong, and I. G. Cumming, "A two-dimensional spectrum for bistatic SAR processing using series reversion," *IEEE Geosci. Remote Sens. Lett.*, vol. 4, no. 1, pp. 93–96, Jan. 2007.

[9] Y. L. Neo, F. H. Wong, and I. G. Cumming, "Processing of azimuth-invariant bistatic SAR data using the range Doppler algorithm," *IEEE Trans. Geosci. Remote Sens.*, vol. 46, no. 1, pp. 14–21, Jan. 2008.

[10] N. Liu, R. Wang, Y. Deng, S. Zhao, and X. Wang, "Modified multichannel reconstruction method of SAR with highly nonuniform spatial sampling," *IEEE J. Sel. Topics Appl. Earth Observ. Remote Sens.*, vol. 10, no. 2, pp. 617–627, Feb. 2017.

[11] M. Rodriguez-Cassola *et al.*, "First bistatic spaceborne SAR experiments with TanDEM-X," *IEEE Geosci. Remote Sens. Lett.*, vol. 9, no. 1, pp. 33–37, Jan. 2012.

[12] G. Krieger, N. Gebert, and A. Moreira, "Unambiguous SAR signal reconstruction from nonuniform displaced phase center sampling," *IEEE Geosci. Remote Sens. Lett.*, vol. 1, no. 4, pp. 260–264, Oct. 2004.

[13] B. Liu and Y. He, "Improved DBF algorithm for multichannel highresolution wide-swath SAR," *IEEE Trans. Geosci. Remote Sens.*, vol. 54, no. 2, p. 1209–1225, Feb. 2016.

[14] H. Gao, J. Chen, S. Quegan, W. Yang, and C. Li, "Parameter estimation and error calibration for multi-channel beam-steering SAR systems," *Remote Sens.*, vol. 11, no. 12, p. 1415, Jun. 2019, doi: 10.3390/rs11121415.

[15] T. Kraus, G. Krieger, M. Bachmann, and A. Moreira, "Spaceborne demonstration of distributed SAR imaging with TerraSAR-X and TanDEM-X," *IEEE Geosci. Remote Sens. Lett.*, vol. 16, no. 11, pp. 1731–1735, Nov. 2019.

[16] T. Kraus, M. Bachmann, and G. Krieger, "Topography correction for distributed SAR imaging: A case study for TerraSAR-X and TanDEM-X," in *Proc. EUSAR*, Jun. 2018, pp. 1–5.

[17] T. Teer and N. A. Goodman, "Multistatic SAR algorithm with image combination," in *Proc. IEEE Conf. Radar*, Apr. 2006, p. 8.

[18] C. E. Yarman, B. Yazici, and M. Cheney, "Bistatic synthetic aperture radar imaging for arbitrary flight trajectories," *IEEE Trans. Geosci. Remote Sens.*, vol. 17, no. 1, pp. 84–93, Jan. 2008.

[19] M. Weiß, "Distributed sensor systems," NATO Lect. Ser., Naples, Italy, Tech. Rep. NATO STO-EN-SET-235, 2017.

[20] L. Iannini *et al.*, "PRF sampling strategies for swarmsar systems," in *Proc. IGARSS-IEEE Int. Geosci. Remote Sens. Symp.*, Yokohama, Japan, Jul. 2019, pp. 8621–8624.

[21] I. Cumming and F. Wong, *Digital Processing of Synthetic Aperture Radar Data: Algorithms and Implementation*. Norwood, MA, USA: Artech House Remote Sensing Library, 2005.

[22] J. L. Brown, "Multi-channel sampling of low-pass signals," *IEEE Trans. Circuits Syst.*, vol. CAS-28, no. 2, pp. 101–106, Feb. 1981.

[23] J. Feng, C. Gao, Y. Zhang, and R. Wang, "Phase mismatch calibration of the multichannel SAR based on azimuth cross correlation," *IEEE Geosci. Remote Sens. Lett.*, vol. 10, no. 4, p. 903–907, Jul. 2013.